Mathematical Biosciences and Engineering

https://www.aimspress.com/journal/mbe

MBE, 22(11): 2923–2943.
DOI: 10.3934/mbe.2025108
Received: 28 May 2025
Revised: 16 August 2025
Accepted: 22 August 2025
Published: 18 September 2025

Research article

Dynamic modeling of internal and external metabolites with energetic and oxidative agents in hyaluronic acid production by *Streptococcus equi* subsp. *zooepidemicus*

Benjamín Angel-Galindo, Rosa Isela Corona-González, Carlos Pelayo-Ortiz and J. Paulo García-Sandoval*

Departamento de Ingeniería Química, CUCEI-Universidad de Guadalajara, Blvd. M. García Barragán 1451, Guadalajara, Jalisco 44430, México

* **Correspondence:** Email: paulo.garcia@academicos.udg.mx.

Abstract: This study presents an ordinary differential equation (ODE) based hybrid kinetic-metabolic model to predict the time evolution of biomass, glucose, hyaluronic acid (HA), and lactic acid during fermentation by *Streptococcus equi* subsp. *zooepidemicus*. The model incorporates simplified metabolic pathways and estimates the qualitative dynamics of internal, unmeasured metabolites involved in glycolysis, biomass synthesis, and HA production. Special emphasis is placed on the energetic molecules ATP/ADP, as well as the coenzymes NADH/NAD^+, which are involved in redox reactions. These molecules have been shown to play regulatory roles in metabolism. The model predictions closely match the experimental data and provide insights into how varying glucose levels affect intracellular metabolic fluxes.

Keywords: hyaluronic acid; modeling; metabolic flux analysis; *Streptococcus equi* subsp. *zooepidemicus*; ATP/ADP and NAD^+/NADH ratios

Abbreviations: HA: Hyaluronic acid; MW: molecular weight; LA: Lactic acid; UDP: Uridine diphosphate; UTP: Uridine triphosphate; ADP: Adenosine diphosphate; ATP: Adenosine triphosphate; HPLC: High performance liquid chromatography; GLU: Glucose; GLE: Extracellular glucose; G6P: Glucose-6-phosphate; F6P: Fructose-6-phosphate; PYR: Pyruvate; PEP: Phosphoenolpyruvate; NAG: UDP-Glucoronic acid; AGL: UDP-N-acetylglucosamine; MSE: Mean squared error.

1. Introduction

Hyaluronic acid (HA), a member of the glycosaminoglycan family [1], is a natural linear copolymer [2] composed of a repeating disaccharide unit of β-1,4-d-glucuronic acid and β-1,3-N-acetylglucosamine joined alternately by glycosidic bonds [3]. Hyaluronan polymers typically contain 500

to 50,000 monosaccharide units per molecule. The polymers have an average molecular weight (MW) of 10^4–10^7 Da [4]. HA is naturally found in vertebrates, bacteria, and mammals. In the human body, HA is abundant in the skin [5], umbilical cord blood [6], intra-articular cartilage [7], skeletal tissues, cardiac valves, aorta, lungs, ear fluid, etc. [8].

HA is a biomaterial with applications in the cosmetic and food industries and the biomedical field. The biomedical uses of HA are vast and include treatments for arthrosis and scars from surgery, aids for cutaneous atrophy and the loss of collagen, plastic surgeries , viscosupplementation, carriers for drug delivery, immune-suppressors, anti-inflammatory agents, etc. [9].

Typically, HA is extracted from the tissues of animals such as rooster combs, and bovines, from which most heavy MW-HA is produced [10]. However, the quantity of tissues from animal sources is scant, the risk of viral infections is high, and the purification steps are costly [11]. Given these limitations, microbial fermentation has emerged as a viable alternative, because the yields are usually higher, the production costs are lower, and the purification processes are more efficient than animal sources [12].

Fermentation is more suitable for large-scale production due to the remarkable productivity of HA using bacterial strains. In particular, *Streptococcus zooepidemicus* is currently used for industrial HA production [12]. However, this fermentation mainly produces lactic acid, which further complicates downstream processing [11]. Optimization represents one of the main challenges in the applied research of HA production, as it is crucial to obtain HA with high-quality control and affordable prices [13].

Mathematical modeling of bioprocesses has a long and remarkable history, with notable contributions from various fields including microbiology, ecology, biophysics, chemistry, statistics, control theory, and mathematical theory [14]. Recently, innovative approaches utilizing "black boxes" such as machine learning, artificial intelligence, and data-driven models have emerged [14]. However, these methodologies often cannot enhance our understanding of the underlying biochemical systems. Bastin and Dochain [15] note that the general state-space model can be complex and may involve numerous differential equations. Nevertheless, there are many practical applications where simplified models suffice. For instance, Rathinavelu et al. [16] introduced a hybrid modeling approach, referred to as a "grey-box" model, which integrates both non-parametric (data-driven) and parametric (mechanistic) elements. This combination serves as a strategic means to address the inherent limitations of either approach when used alone [17].

In the context of production, mathematical models can significantly deepen our understanding of the underlying systems and help identify potential improvements in the production processes. Existing models for HA production encompass various methodologies, including those based on mass balance equations, neural network frameworks, and metabolic flux calculations that use stoichiometric invariances derived from metabolic pathway analysis. Modeling cellular metabolism is essential in biotechnology and metabolic engineering, as these models can facilitate the enhancement of current production methods and support the development of new processes [18].

The most widely studied models for HA production are those grounded in mass balance equations, which consider global kinetics using approximate bioreaction rates, similar to the Monod or Haldane models, to capture the dynamics of observable species, such as substrates, products, and biomass. Several researchers, including Don and Shoparwe [19], Vázquez et al. [20], Amado et al. [21], Ozcan et al. [22], and Rohit et al. [23], have proposed logistic equations to model HA production by

S. zooepidemicus using various carbon sources such as glucose, sucrose, or molasses. For instance, Don and Shoparwe [19] utilized an integrated Luedeking-Piret type equation to model HA production alongside cellular growth and glucose consumption with *S. zooepidemicus* ATCC 39920, while Ozcan et al. [22] analyzed the Luedeking-Piret model and its modified version. Liu et al. [24] explored a Monod-type kinetic model to describe the cell growth rates and HA formation from sucrose. Recently, Flores-Méndez et al. [25] introduced a mathematical model which utilized the Haldane-Egamberdiev kinetic law and elucidated how glucose inhibition affects specific rates, with lactic acid having a particularly detrimental effect on both cell growth and HA production. An alternative approach involves artificial neural networks, where differential equations link specific rate parameters to state variables, thus allowing for predictive modeling of the HA concentration. Liu et al. [26] advanced this approach by modeling the effect of amino acid supplementation on HA production in *S. zooepidemicus* using a quantum particle swarm optimization algorithm alongside a radial basis function neural network.

While mathematical models for HA production have the potential to enhance our understanding of metabolic processes and suggest improvements, there is a notable scarcity of comprehensive studies in this area. Such models provide valuable insights to systematically explore the complex topology of metabolic pathways; however, understanding the kinetics of these pathways is equally essential. Cooney et al. [27] developed an extended structured two-compartment model that considered two substrates and multi-product HA fermentation under conditions of both anaerobic and aerobic growth. The model utilized the synthesizing components of the cell (ribosomes, mRNA, tRNA, various enzymes, etc.), in which the primary constituent was the protein-synthesizing system, made up of about 60% RNA. The two-compartment model framework was found to be robust, easily adaptable, and capable of predicting the transient consumption of substrates and the formation of products. Similarly, Shah et al. [28] analyzed metabolic flux at different levels of glycolytic pathway inhibition to understand its effect on flux distribution in the metabolic network. Fong Chong and Nielsen [29] constructed a metabolic flux model aimed at estimating intracellular fluxes and validating the measurement consistency, with a focus on key pathways including the Embden-Meyerhof-Parnas pathway, the pentose phosphate pathway, and the reactions responsible for the formation of fermentation products (lactate, formate, acetate, ethanol, N-acetylglucosamine, and glucuronic acid) in *S. zooepidemicus*. Their work evaluated the metabolic flux from glucose and maltose substrates. Additionally, Gao et al. [30] conducted a metabolic network analysis based on the quasi-steady-state hypothesis, which estimated the distribution of metabolic network flow according to the stoichiometric ratio of each reaction in the metabolic pathway at different stages and culture conditions.

In conclusion, while various mathematical modeling approaches have been applied to enhance HA production, further investigation into the synergies between mechanistic and data-driven models, particularly regarding their integration and potential limitations, is essential to advance the field. Identifying these gaps may lead to improved modeling techniques and, subsequently, a better understanding of the production process itself. In our current work, we develop and test a mathematical model that integrates kinetic and metabolic pathways approaches to predict the dynamic behavior of measured substrate, biomass, and product concentrations. The model considers the qualitative dynamic behavior of unmeasured internal metabolites, including both energetic molecules ATP/ADP, as well as the coenzymes NADH/NAD^+, which are involved in redox reactions. These molecules have been shown to play regulatory roles in metabolism.

2. Materials and methods

2.1. Fermentations data set

Flores-Méndez et al. [25] performed experiments to analyze the effect of different initial concentrations of glucose and lactic acid (LA) on *S. zooepidemicus* biomass growth and HA production (see Figure 1). In the present work, we used this experimental data set to test our proposed mathematical model.

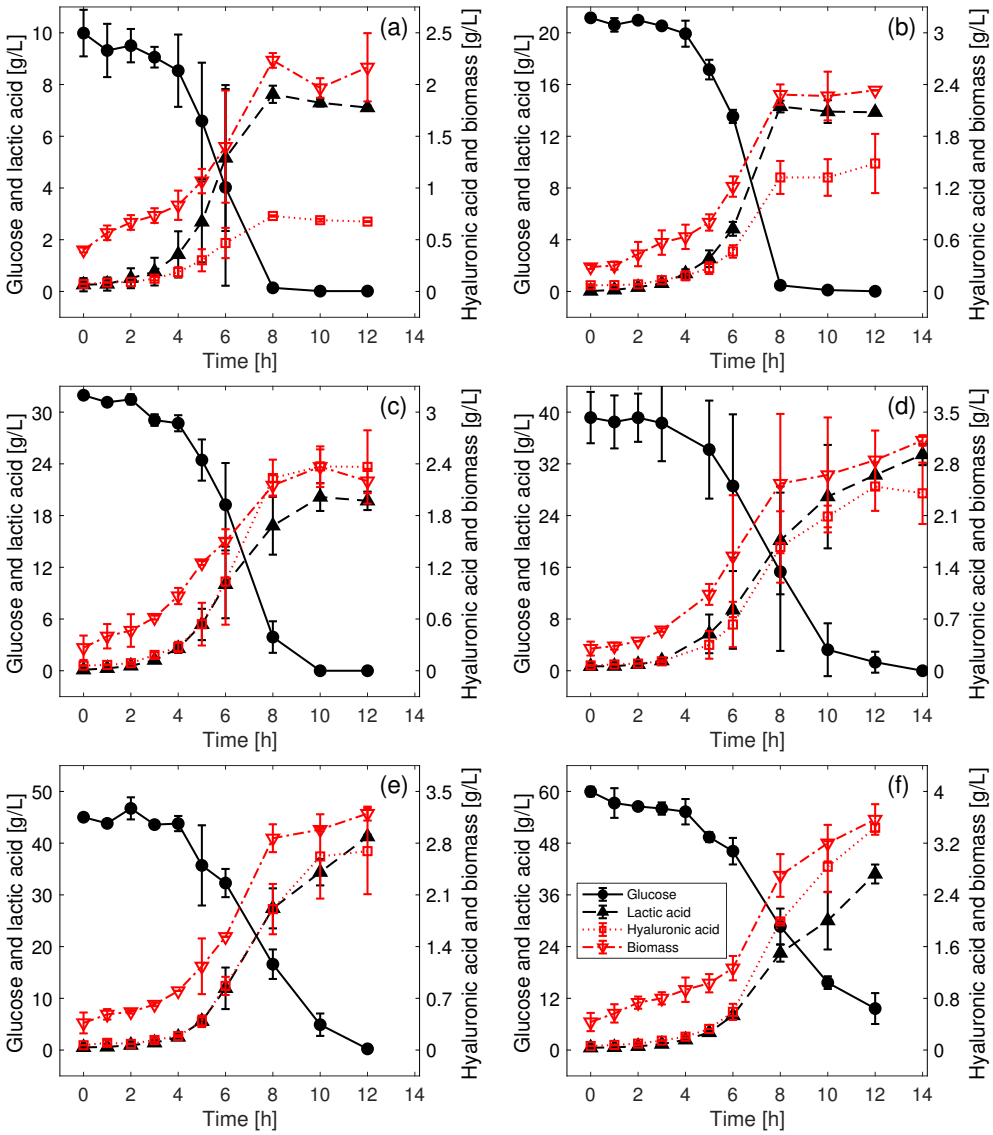

Figure 1. Experimental data for glucose (■), lactic acid (▲), hyaluronic acid (□), and biomass (▽). Initial glucose concentration of: (a) **Experiment 1:** 9.3 g/L, (b) **Experiment 2:** 21.1 g/L, (c) **Experiment 3:** 31.9 g/L, (d) **Experiment 4:** 39.1 g/L, (e) **Experiment 5:** 45.5 g/L, and (f) **Experiment 6:** 59.9 g/L.

The experimental conditions used by Flores-Méndez et al. [25] is summarized below:
Inoculum: *Streptococcus equi* subsp. *zooepidemicus* ATCC 35246 was inoculated (10% v/v) in

the reactor production medium. **Batch Fermentation:** Batch cultures were grown at 37 °C, 300 rpm, pH of 7, one vvm airflow, and 5% dissolved oxygen in a working volume of 2 L. The culture medium consisted of the following yeast extract (10 g/L); NaCl (2 g/L); K_2HPO_4 (2.5 g/L); $MgSO_4 \cdot 7\,H_2O$ (2.5 g/L); and glucose with varying initial concentrations (**Experiment 1:** 9.3 g/L, **Experiment 2:** 21.1 g/L, **Experiment 3:** 31.9 g/L, **Experiment 4:** 39.1 g/L, **Experiment 5:** 45.5 g/L, and **Experiment 6:** 59.9 g/L). **Analysis methods:** The biomass content was determined by the dry weight, while HA, glucose, and organic acids were quantified by high performance liquid chromatography (HPLC). Further details can be found in [25].

2.2. *Mathematical modeling*

2.2.1. Simplified pathways

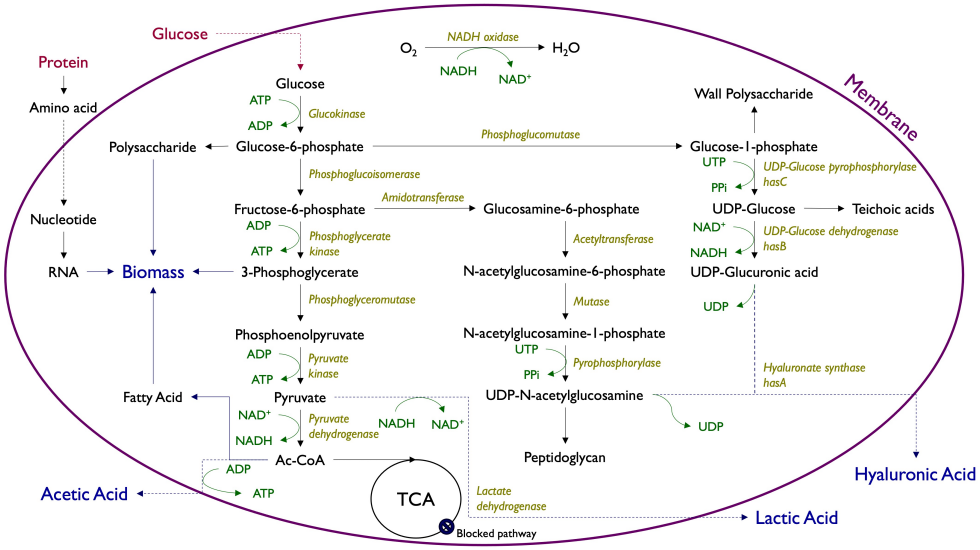

Figure 2. The biological synthesis pathway of hyaluronic acid in *Streptococcus zooepidemicus*. Modified from [31].

Figure 2 shows the HA biosynthetic pathway in *S. zooepidemicus* alongside simplified pathways of biomass growth, acetic acid and LA production from glucose and proteins. In *S. zooepidemicus*, HA is produced from the precursors uridine diphosphate (UDP)-glucuronic acid and UDP-N-acetylglucosamine [5]. HA is mainly synthesized in the plasma membranes by HA synthase [7], which is an enzyme that catalyzes the polymerization of both substrates [3]. The journey of HA biosynthesis commences with the phosphorylation of glucose by hexokinase, which leads to the production of glucose-6-phosphate (G6P). Then, the synthesis pathway bifurcates into two distinct routes [4], which is similar to what occurs for the metabolism of carbohydrates in purple non-sulfur bacteria (PNSB), where the G6P either goes to the Embden-Meyerhof-Parnas pathway in both metabolic pathways or to the Entner-Doudoroff pathway, where it becomes 6-phosphogluconate, which goes to the pentose phosphate pathway (oxidative phase and then non oxidative phase) in the PNSB [32]. Meanwhile, in our study, it diverges in the HA synthesis pathway, which can be divided into two sets. In the first set of reactions, G6P metamorphoses into glucose-1-phosphate. UDP-glucose pyrophosphorylase steps in, which adds UTP to glucose-1-phosphate, culminating in the production of

UDP-glucose [31]. Finally, thanks to the mediation of UDP-glucose dehydrogenase, UDP-glucose undergoes oxidation to transform into UDP-glucuronic acid. In the second pathway, phosphoglucoisomerase facilitates the transfer of G6P to fructose-6-phosphate (F6P); then, an amido group is added to yield glucosamine-6-phosphate [4]. A phosphate group rearrangement by phosphoglucosamine mutase produces glucosamine-1-phosphate. The acetylated form of this compound is created in the next step by phosphoglucosamine acetyltransferase. Finally, N-acetylglucosamine-1-phosphate pyrophosphorylase activates the intermediate by adding UTP, which yields the second HA precursor, UDP-N-acetylglucosamine [33]. After synthesizing the two precursors, HA synthase polymerizes them to produce the HA polymer [4].

Showing similar results, Klamt et al. [34] worked with a kinetic model of a stoichiometric reaction network composed of only seven reactions. They focused either on purely respiratory or purely photosynthetic growth, where the main activity of the electron transport chain (ETC) was located either exclusively in the cytoplasmic membrane or the intracytoplasmic membranes. They argue that a compartmentalized model would not change the main results and found that the stoichiometric model could only show the potential behavior of the ETC. They had to include regulatory pathways within the model to study the driving forces, electron flows, and redox states under different conditions.

As depicted in Figure 2, the HA production is a complex process that involves several steps inside microorganisms. To model this complex system, we start with a simplified version of this metabolic pathway, shown in Figure 3, whose overall reactions are given in Table 1, where intermediate reactions have been grouped to obtain the overall reactions containing bifurcation points for some reactants or products. In general, the simplified pathway can be split into three groups of reactions: 1) **R1**, **R2**, **R3**, **R4**, and **R5** are associated to glucose metabolism; 2) **R6**, **R7**, and **R8** are associated to HA production; and 3) **R9** and **R10** describe the biomass growth. In particular, reaction **R1** describes the transformation of intracellular glucose (GLU) to G6P mediated by glucokinase and one ATP, while **R2** represents the G6P reaction to produce F6P mediated by phosphoglucoisomerase. On the other hand, the consecutive reactions of F6P to 3-phosphoglycerate to phosphoenolpyruvate (PEP) are grouped in only one overall reaction described by **R3**, while **R4** describes the reaction of PEP to produce pyruvate (PYR) mediated by pyruvatekinase and one ADP. The transformation of PYR to LA mediated by lactate dehydrogenase and NADH is represented by **R5**, while the precursors of HA are obtained in **R6** and **R7**. In particular, **R6** condensates the reactions of F6P to glucosamine-6-phosphate to N-acetylglucosamine-6-phosphate to N-acetylglucosamine-I-phosphate to UDP-N-acetylglucosamine (AGL) in only one overall reaction, while **R7** groups the reactions of G6P to glucose-I-phosphate to UDP-Glucose to UDP-Glucoronic acid (NAG). These two pathways require UTP and produce UDP; However, to simplify the model and reduce the number of species, we consider ATP and ADP instead. Finally, **R8** describes HA production from AGL and NAG, while the biomass can be produced by two pathways, **R9** and **R10**, from G6P and PEP together with PYR and NAD^+, respectively. All reactions in Table 1 are balanced in molar units. However, the biomass shown in reactions **R9** and **R10** are in mass units, since the exact apparent MWs for the microorganisms are not available; additionally, it is unknown how much G6P and PEP are consumed per mole of NAD^+ consumed, since proteins, lipids, and other compounds are also involved in cell growth. Thus, reactions **R1** to **R8** have well-established stoichiometric coefficients, while **R9** and **R10** have biomass growth yield coefficients (i.e., $Y_{\mathrm{G6P/PYR}}$ and $Y_{\mathrm{G6P/X}}$ for **R9**, and $Y_{\mathrm{PEP/PYR}}$ and $Y_{\mathrm{PEP/X}}$ and $Y_{\mathrm{G6P/X}}$ for **R10**, respectively).

Table 1. Simplified overall reactions inside the cells.

GLU + ATP	$\longrightarrow$	G6P + ADP	**(R1)**
G6P	$\longrightarrow$	F6P	**(R2)**
F6P + ADP + 2NAD$^+$	$\longrightarrow$	2PEP + ATP + 2NADH	**(R3)**
PEP + ADP	$\longrightarrow$	PYR + ATP	**(R4)**
PYR + NADH	$\longrightarrow$	LA + NAD$^+$	**(R5)**
G6P + ATP + NAD$^+$	$\longrightarrow$	AGL + NADH	**(R6)**
F6P + ATP	$\longrightarrow$	NAG	**(R7)**
AGL + NAG	$\longrightarrow$	HA + 2ADP	**(R8)**
$Y_{\text{G6P/PYR}}$G6P + PYR + NAD$^+$	$\longrightarrow$	$Y_{\text{G6P/X}}$X + NADH	**(R9)**
$Y_{\text{PEP/PYR}}$PEP + PYR + NAD$^+$	$\longrightarrow$	$Y_{\text{PEP/X}}$X + NADH	**(R10)**

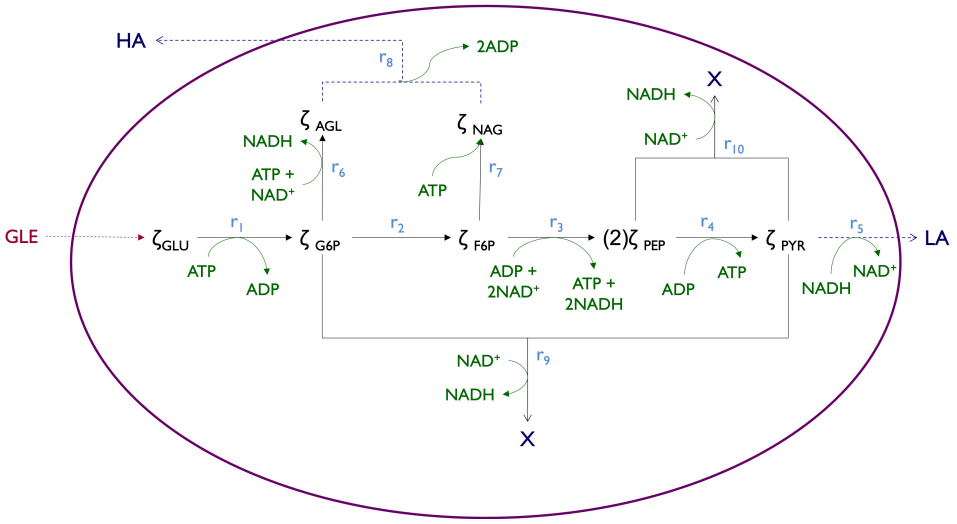

Figure 3. Simplified metabolic pathway.

2.2.2. Balances

To model the dynamical behavior of biomass growth, glucose consumption, HA, and LA production, we proposed a semi-structured model based on mass balances that takes the simplified metabolic pathway presented in the previous subsection into account. To achieve this goal, we consider the following assumptions:

A1. The extracellular glucose (GLE) enters the cells by facilitated diffusion.

A2. The biomass concentration, [X], as well as the extracellular concentrations of glucose, [GLE], hyaluronic acid, [HA], and lactic acid, [LA], are measured and well known, while the intracellular concentrations are unmeasured; therefore, instead of using mass or molar concentrations, we used the following internal variables: ζ_{GLU}, ζ_{G6P}, ζ_{F6P}, ζ_{PEP}, ζ_{PYR}, ζ_{AGL}, ζ_{NAG}, ζ_{ATP}, ζ_{ADP}, ζ_{NADH}, and ζ_{NAD^+}, which are correlated with (but not necessarily equal to) the intracellular molar concentrations of glucose, glucose-6-phosphate, fructose-6-phosphate, phosphoenolpyruvate, pyruvate, UDP-N-acetylglucosamine, UDP-Glucoronic acid, ATP, ADP, NADH, and NAD$^+$, respectively.

A3. Under the operational conditions, the intracellular biochemical reactions described in Table 1 only take place in one direction (i.e., they can be considered to be irreversible), and the specific reaction rates, r_i for $i = 1, 2, \ldots, 10$, can be expressed with elementary kinetics. This assumption comes from the fact that most of the reactions depicted in Figure 2 are enzyme-catalyzed and are part of larger unidirectional cycles, such as Krebs' cycle.

A4. The sum of intracellular phosphorated metabolites (i.e., ATP, ADP, AGL, and NAG) and the sum of the intracellular metabolites (i.e., NADH and NAD^+) are proportional to the biomass concentration. Thus, if the biomass grows, then the amount of these metabolites also increases proportionally. In particular, we assume that when the biomass grows, the metabolites that increase inside the cells are both ADP and NAD^+.

Taking the Assumptions **A1**–**A4** into account, the mass balances of the extracellular concentrations, the biomass, and the internal variables are as follows:

$$\frac{d\,[\mathrm{GLE}]}{dt} = -J_{\mathrm{GL}}, \tag{2.1}$$

$$\frac{d\,[\mathrm{LA}]}{dt} = r_5, \tag{2.2}$$

$$\frac{d\,[\mathrm{HA}]}{dt} = r_8, \tag{2.3}$$

$$\frac{d\,[\mathrm{X}]}{dt} = Y_{\mathrm{G6P/X}} r_9 + Y_{\mathrm{PEP/X}} r_{10} - k_D\,[\mathrm{X}]\,, \tag{2.4}$$

$$\frac{d\zeta_{\mathrm{GLU}}}{dt} = -r_1 + J_{\mathrm{GL}}, \tag{2.5}$$

$$\frac{d\zeta_{\mathrm{G6P}}}{dt} = r_1 - r_2 - r_6 - Y_{\mathrm{G6P/PYR}} r_9, \tag{2.6}$$

$$\frac{d\zeta_{\mathrm{F6P}}}{dt} = r_2 - r_3 - r_7, \tag{2.7}$$

$$\frac{d\zeta_{\mathrm{PEP}}}{dt} = 2r_3 - r_4 - Y_{\mathrm{PEP/PYR}} r_{10}, \tag{2.8}$$

$$\frac{d\zeta_{\mathrm{PYR}}}{dt} = r_4 - r_5 - r_9 - r_{10}, \tag{2.9}$$

$$\frac{d\zeta_{\mathrm{AGL}}}{dt} = r_6 - r_8, \tag{2.10}$$

$$\frac{d\zeta_{\mathrm{NAG}}}{dt} = r_7 - r_8, \tag{2.11}$$

$$\frac{d\zeta_{\mathrm{ATP}}}{dt} = -r_1 + r_3 + r_4 - r_6 - r_7, \tag{2.12}$$

$$\frac{d\zeta_{\mathrm{NADH}}}{dt} = 2r_3 - r_5 + r_6 + r_9 + r_{10}, \tag{2.13}$$

where J_{GL} is the specific flow of extracellular glucose into the cells, which, according to Assumption **A1**, is given by

$$J_{\mathrm{GL}} = k_G\,([\mathrm{GLE}] - m\zeta_{\mathrm{GLU}})\,, \tag{2.14}$$

where k_G is the glucose diffusion coefficient, and m is an intra-extracellular glucose equilibrium constant associated to the facilitated diffusion.

Due to Assumption **A3**, the kinetic rates are as follows:

$$\begin{aligned} r_1 &= k_1\zeta_{\mathrm{GLU}}\zeta_{\mathrm{ATP}}, && (2.15)\\ r_2 &= k_2\zeta_{\mathrm{G6P}}, && (2.16)\\ r_3 &= k_3\zeta_{\mathrm{F6P}}\zeta_{\mathrm{ADP}}\zeta^2_{\mathrm{NAD^+}}, && (2.17)\\ r_4 &= k_4\zeta_{\mathrm{PEP}}\zeta_{\mathrm{ADP}}, && (2.18)\\ r_5 &= k_5\zeta_{\mathrm{PYR}}\zeta_{\mathrm{NADH}}, && (2.19)\\ r_6 &= k_6\zeta_{\mathrm{G6P}}\zeta_{\mathrm{NAD^+}}\zeta_{\mathrm{ATP}}, && (2.20)\\ r_7 &= k_7\zeta_{\mathrm{F6P}}\zeta_{\mathrm{ATP}}, && (2.21)\\ r_8 &= k_8\zeta_{\mathrm{AGL}}\zeta_{\mathrm{NAG}}, && (2.22)\\ r_9 &= k_9\zeta_{\mathrm{PYR}}\zeta_{\mathrm{G6P}}\zeta_{\mathrm{NAD^+}}, && (2.23)\\ r_{10} &= k_{10}\zeta_{\mathrm{PYR}}\zeta_{\mathrm{PEP}}\zeta_{\mathrm{NAD^+}}, && (2.24) \end{aligned}$$

where k_i for $i = 1, 2, \ldots, 10$ are the specific reaction rate constants. In addition, due to Assumption **A4**, the following must hold:

$$\begin{aligned} \alpha\,[\mathrm{X}] &= \zeta_{\mathrm{ATP}} + \zeta_{\mathrm{ADP}} + \zeta_{\mathrm{AGL}} + \zeta_{\mathrm{NAG}}, && (2.25)\\ \beta\,[\mathrm{X}] &= \zeta_{\mathrm{NADH}} + \zeta_{\mathrm{NAD^+}}, && (2.26) \end{aligned}$$

where α and β are constants of proportionality. Notice that considering the balances for the biomass, AGL, NAG, and ATP described in Eqs 2.4, 2.10, 2.11, and 2.12, respectively, and the proportionality of Eq 2.25, the balance for ζ_{ADP} has the form:

$$\frac{d\zeta_{\mathrm{ADP}}}{dt} = r_1 - r_3 - r_4 + 2r_8\alpha Y_{\mathrm{G6P/X}} r_9 + \alpha Y_{\mathrm{PEP/X}} r_{10} - k_D\alpha\,[\mathrm{X}]\,. \tag{2.27}$$

Similarly, considering the balances for the biomass and NADH described in Eqs 2.4 and 2.13, respectively, and the proportionality of Eq 2.26, the balance for $\zeta_{\mathrm{NAD^+}}$ is as follows:

$$\frac{d\zeta_{\mathrm{NAD^+}}}{dt} = -2r_3 + r_5 - r_6 - \left(1 - \beta Y_{\mathrm{G6P/X}}\right) r_9 - \left(1 - \beta Y_{\mathrm{PEP/X}}\right) r_{10} - k_D\beta\,[\mathrm{X}]\,. \tag{2.28}$$

Therefore, Assumption **A4** is fulfilled, because the metabolites that increase inside the cells are ADP and $\mathrm{NAD^+}$ when the biomass grows.

In summary, the proposed model is composed of the balances given in Eqs 2.1–2.13, 2.27, and 2.28, the glucose transport in Eq 2.14, and the reaction rates given in Eqs 2.15 and 2.16. This model contains 19 parameters: ten specific reaction rate constants, k_i for $i = 1, 2, 3, \ldots, 10$, two glucose's diffusion coefficients, k_G and m, four growth yield coefficients, $Y_{\mathrm{G6P/X}}$, $Y_{\mathrm{G6P/PYR}}$, $Y_{\mathrm{PEP/X}}$, and $Y_{\mathrm{PEP/PYR}}$, two proportionality coefficients, α and β, and one coefficient associated to biomass death, k_D.

Under the assumption of a quasi-steady state for the dynamic of the internal variables (i.e., ζ_{GLU}, ζ_{G6P}, ζ_{F6P}, ζ_{PEP}, ζ_{PYR}, ζ_{AGL}, ζ_{NAG}, ζ_{ATP}, and ζ_{NADH}), the proposed model given in Eqs 2.1–2.13 reduces to the following (see the section A of the Supplementary material for further detail):

$$\begin{pmatrix} \frac{d[\mathrm{GLE}]}{dt} \\ \frac{d[\mathrm{LA}]}{dt} \\ \frac{d[\mathrm{HA}]}{dt} \\ \frac{d[\mathrm{X}]}{dt} \end{pmatrix} = \begin{pmatrix} -1 \\ Y_{\mathrm{LA/GLE}} \\ Y_{\mathrm{HA/GLE}} \\ Y_{\mathrm{X/GLE}} \end{pmatrix} k_1 \frac{[\mathrm{GLE}]}{m + \frac{k_1}{k_G}\zeta_{\mathrm{ATP}}} \zeta_{\mathrm{ATP}} - \begin{pmatrix} 0 \\ 0 \\ 0 \\ k_D\,[\mathrm{X}] \end{pmatrix}. \tag{2.29}$$

Therefore, under the assumption of a quasi-steady state for the intracellular dynamics, the proposed model has only one reaction rate, $r_1 = k_1 \frac{[\mathrm{GLE}]}{m+\frac{k_1}{k_G}\zeta_{\mathrm{ATP}}}\zeta_{\mathrm{ATP}}$, and variable biomass, LA, and HA yield coefficients, $Y_{\mathrm{LA/GLE}} = Y_{\mathrm{LA/GLE}}(\zeta_{\mathrm{NAD^+}}\zeta_{\mathrm{ATP}})$, $Y_{\mathrm{LA/GLE}} = Y_{\mathrm{LA/GLE}}(\zeta_{\mathrm{NAD^+}}\zeta_{\mathrm{ATP}})$, and $Y_{\mathrm{X/GLE}} = Y_{\mathrm{X/GLE}}(\zeta_{\mathrm{NAD^+}}\zeta_{\mathrm{ATP}})$, respectively, that depend on the energetic and oxidative state of the microorganisms. According to the model, these can vary with the initial state of the microorganisms and the external glucose concentration. Due to the relations given in Eqs 2.25 and 2.26, ζ_{ATP} is proportional to a fraction of the biomass concentration and reflects the energetic state inside the cells. Therefore, r_1 has the following limit cases for the glucose consumption: when the cells have sufficient energy, in such a way that $\zeta_{\mathrm{ATP}} \gg k_G m/k_1$, the rate of glucose consumption approaches to $r_1 = k_G\,[\mathrm{GLE}]$ and only depends on the rate of glucose absorption; and for small cells' energy (i.e., $\zeta_{\mathrm{ATP}} \ll k_G m/k_1$), it holds that $r_1 = \frac{k_1}{m}[\mathrm{GLE}]\,\zeta_{\mathrm{ATP}} \propto [\mathrm{GLE}]\,[\mathrm{X}]$, thus resembling a Monod-type saturation in the reaction rate, which depends on the energy state of the microorganisms. Obviously, without the assumption of a quasi-steady state, the proposed model can have a reacher behavior than what is described by Eq 2.29.

3. Results and discussion

3.1. Model predictions

In this work, we introduce a new approach to model the production of HA that considers kinetic and metabolic pathways approaches. Diverging from Rathinavelu et al. [16], we present a unique parametric model (based on data) that incorporates the process's biochemistry and includes logical considerations and mechanisms specific to the bacterial cell wall. Experimental data from experiments 1, 2, 4, and 6 were used to estimate the parameters of the proposed model. The fitting procedure was performed with a least squares method using the Nealder-Mead minimization algorithm [35] (see Sections B of the Supplementary material for further detail). Table 2 shows the values of the obtained parameters and their confidence intervals [36]. This model demonstrates a mere 0.0278% difference between the data and the proposed model, a result well within their reported range.

The consistency of predictions and experiments conducted at several initial glucose concentrations demonstrate the robustness of our model and underscores the reliability of our approach. However, the mean squared error (MRE) value decreases as the glucose concentration increases. In experiments 1 through 6, the MSE values are 0.0508, 0.0310, 0.0266, 0.0221, 0.0201, and 0.0163, respectively. This fact could reflect a problem with the proposed model at low concentrations, though it may also be a problem correlated with the increased uncertainty in the experimental data, as seen in the error bars in plots (a,b,c,d-1) of Figure 4.

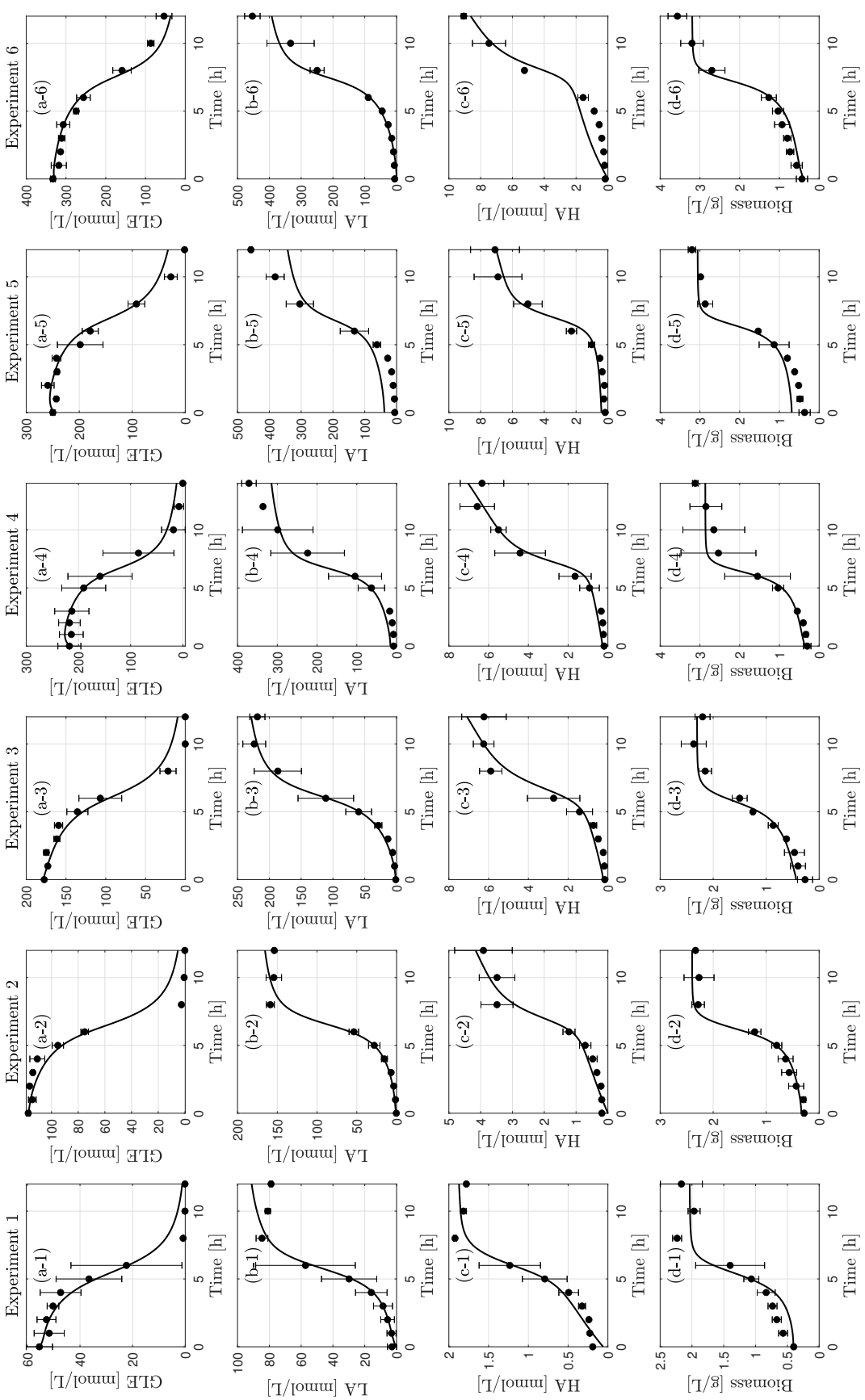

Figure 4. Comparison of experimental data and model predictions.

Table 2. Model parameters and their confidence interval.

Parameter	Value	Parameter	Value
	Glucose diffusion coefficients		
k_G	$0.7432 \pm 0.1716\,\mathrm{h}^{-1}$	m	$1.297 \pm 5.391 \times 10^{-2}$
	Kinetic constants		
k_1	$1.128 \pm 6.637 \times 10^{-3}\ \frac{\mathrm{L}}{\mathrm{mmol \cdot h}}$	k_2	$0.8348 \pm 2.505 \times 10^{-1}\,\mathrm{h}^{-1}$
k_3	$1.187 \times 10^{-3} \pm 3.009 \times 10^{-4}\ \frac{\mathrm{L}^3}{\mathrm{mmol}^3 \cdot \mathrm{h}}$	k_4	$10.86 \pm 6.086 \times 10^{-3}\ \frac{\mathrm{L}}{\mathrm{mmol \cdot h}}$
k_5	$4.631 \times 10^{-2} \pm 4.439 \times 10^{-3}\ \frac{\mathrm{L}}{\mathrm{mmol \cdot h}}$	k_6	$6.515 \times 10^{-2} \pm 4.962 \times 10^{-2}\ \frac{\mathrm{L}^2}{\mathrm{mmol}^2 \cdot \mathrm{h}}$
k_7	$2.906 \times 10^{-3} \pm 2.252 \times 10^{-3}\ \frac{\mathrm{L}}{\mathrm{mmol \cdot h}}$	k_8	$2.951 \times 10^{-2} \pm 1.162 \times 10^{-4}\ \frac{\mathrm{L}}{\mathrm{mmol \cdot h}}$
k_9	$9.345 \times 10^{-5} \pm 2.752 \times 10^{-4}\ \frac{\mathrm{L}^2}{\mathrm{mmol}^2 \cdot \mathrm{h}}$	k_{10}	$0.2077 \pm 1.175 \times 10^{-1}\ \frac{\mathrm{L}^2}{\mathrm{mmol}^2 \cdot \mathrm{h}}$
k_D	$0 \pm 2.985 \times 10^{-3}\,\mathrm{h}^{-1}$		
	Energetic and oxidative proportion		
α	$29.10 \pm 1.022 \times 10^{-2}\ \frac{\mathrm{mmol}}{\mathrm{g}}$	β	$41.07 \pm 4.670 \times 10^{-2}\ \frac{\mathrm{mmol}}{\mathrm{g}}$
	Growth yield coefficients		
$Y_{\mathrm{G6P/X}}$	$3.260 \times 10^{-4} \pm 9.623 \times 10^{-2}\ \frac{\mathrm{g}}{\mathrm{mmol}}$	$Y_{\mathrm{PEP/X}}$	$0.2351 \pm 1.289 \times 10^{-1}\ \frac{\mathrm{g}}{\mathrm{mmol}}$
$Y_{\mathrm{G6P/PYR}}$	$0.2009 \pm 1.603 \times 10^{-3}\ \frac{\mathrm{g}}{\mathrm{mmol}}$	$Y_{\mathrm{PEP/PYR}}$	$1.184 \pm 6.180 \times 10^{-2}\ \frac{\mathrm{g}}{\mathrm{mmol}}$

The values of the kinetic parameters obtained when adjusting the proposed model (see Table 2) are of utmost importance. Notably, k_G is 0.7432 h^{-1}, which indicates efficient glucose consumption, a characteristic of a bacteria whose feeding is by facilitated diffusion. Furthermore, k_D is of the order of 10^{-23} h^{-1}, which is a value so small that it is negligible, thus suggesting that cell death (due to lysis or some other cause) was insignificant. Most parameters have a low correlation with each other and a conservative confidence interval, except those associated with reactions **R9** and **R10** of biomass growth and, to a lesser extent, reactions **R6** and **R7** associated with HA production (see Sections B of the Supplementary material).

The value of α is 29% times smaller than β, which shows a lower presence of ATP/ADP inside the cell than of NAD^+/NADH. In the literature, Buchholz et al. [37] reported the opposite, namely a 60% increased presence of ADP /ATP compared to NAD^+/NADH; thus, it should be considered that it is a different microorganism and that no reports of the bacteria *Streptococcus equi* subsp. *zooepidemicus* were found. Zbornikova et al. [38] measured these metabolites in *E. coli,* and there was 4.7 times more NAD^+/NADH activity than ATP/ADP for mucopyrin (+) strains. The opposite happened with mucopyrin (-) strains, in which the ATP/ADP ratio was 3.2 times greater than NAD^+/NADH.

Figure 4 compares the resulting model predictions and the experimental data of glucose consumption, LA and HA production, and biomass growth. In all cases, how the model correlates with each behavior is very noticeable, thus presenting a minimal difference in some points. The figure shows that the maximum LA production was in experiment 5 at 12 h with 41.2 g/L. For HA, the maximum production was in experiment 6 at 12 h with 3.4 g/L. It is important to remark that experiments 3 and 5 were not used to fit the model; therefore, these experiments can be used to validate the model's predictability under experimental conditions different from those used in its fitting.

One feature of the proposed model is the prediction of the qualitative behavior of internal metabolites. To analyze these internal metabolites, let us define the amount of internal metabolites per units of biomass as $x_{\mathrm{GLU}} = \zeta_{\mathrm{GLU}}/X$, $x_{\mathrm{G6P}} = \zeta_{\mathrm{G6P}}/X$, $x_{\mathrm{F6P}} = \zeta_{\mathrm{F6P}}/X$, $x_{\mathrm{PEP}} = \zeta_{\mathrm{PEP}}/X$, $x_{\mathrm{PYR}} = \zeta_{\mathrm{PYR}}/X$,

$x_{AGL} = \zeta_{AGL}/X$, $x_{NAG} = \zeta_{NAG}/X$, $x_{ATP} = \zeta_{ATP}/X$, $x_{ADP} = \zeta_{ADP}/X$, $x_{NADH} = \zeta_{NADH}/X$, and $x_{NAD^+} = \zeta_{NAD^+}/X$. The behaviors derived from the model for intracellular GLU, G6P, and F6P (x_{GLU}, x_{G6P}, and x_{F6P}) are plotted in the first row of Figure 5 (plots (a-1)–(a-6)). GLU shows the same consumption behavior as that observed in the six experiments. As GLU transforms into G6P, the consumption crossover from one generation to the other is evident in the six experiments, with G6P presenting a peak at the stage when GLU is abruptly consumed. Subsequently, G6P becomes F6P, which is why F6P presents a generational behavior throughout the six experiments.

F6P undergoes a series of transformations to reach PEP. One of those conversions involves splitting the molecule from C6 to C3, thus doubling the number of moles. In the second row of Figure 5 (plots (b-1)–(b-6)), we can see the behavior of PEP and its product, PYR (x_{PEP} and x_{PYR}). Both present similar graphs, with a peak in the exponential phase because it is the stage in which the bacteria produce these metabolites in excess. They will serve as a supply to produce biomass and LA. In the specific case of PEP in experiments 3, 4, and 6, the model shows a slight peak in the latency phase; this generation of excess PEP will serve the microorganism for cell replication in the exponential phase.

The central row of Figure 5 (plots (c-1)–(c-6)) shows the graphs of the model for the behavior of AGL and NAG (x_{AGL} and x_{NAG}); remembering that HA is composed of equimolar chains of both components, it is observed that there is more significant activity in AGL, which represents an overproduction of one of the two. In fact, in the six experiments, NAG was consumed in its entirety. Therefore, it is considered the limiting reagent in the fermentative production of HA.

From Figure 5(a-1) to (a-6), for all initial glucose concentrations, the consumption of glucose (GLU) is total; the concentration of G6P increases, reaches the highest concentration around 7 hours, and then decreases. While F6P accumulates during the run, the final concentration of F6P increases as the initial glucose concentration increases. This is explained because glucose is transformed to G6P during glycolysis and can take either the path toward the formation of polysaccharides of biomass or undergo conversion to glucose-1-phosphate, then to UDP-glucose, then UDP-glucuronic acid (NAG), which is the first precursor of HA. In contrast, fructose is converted to glucosamine-6-phosphate to form UDP-N-acetylglucosamine (NAG) that goes to straight the formation of glycopeptide and, therefore, to the formation of biomass [9, 31, 39]. Since the biomass does not significantly increase (2–3 g/L) with an increasing initial glucose concentration (10–60 g/L), F6P is not converted to biomass; therefore, it remains as F6P, and its concentration increases over time and with an increasing initial glucose concentration.

The fourth row of Figure 5 (plots (d-1)–(d-6)) illustrates the behavior of metabolites associated with primary energy, as per the proposed model (x_{ATP} and x_{ADP}). Two curves are depicted: ADP exhibits a peak in the exponential phase that diminishes in the stationary phase, while ATP remains nearly at zero, thus indicating no accumulation in the latency phase. In the exponential phase, ATP shows a slight peak, which is consumed in the stationary phase.

The biosynthesis of hyaluronate in *streptococci* demands high energy, which competes against cell growth for glucose as either an energy provider or precursor of sugar-UDP. It has been observed that when glucose is limited, the bacterial growth is higher in optimal culture conditions (i.e., at pH 7 and 37 °C). In contrast, productivity and a higher MW of hyaluronate are obtained at sub-optimal growth conditions because carbon and energetic resources are available for other processes when cells grow slowly. By limiting the glucose conditions, the hyaluronate productivity decreases, followed by the MW [8, 39].

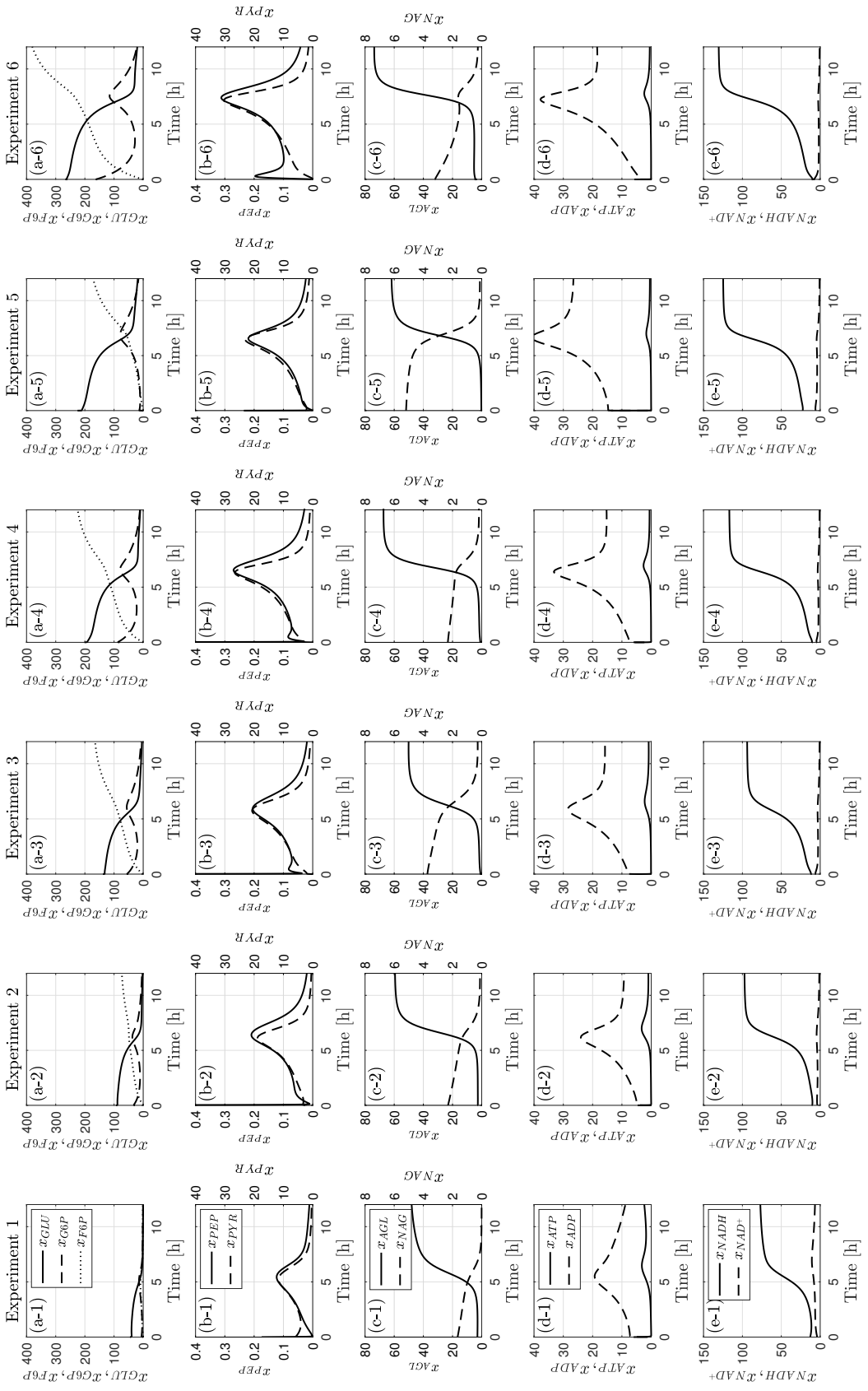

Figure 5. Amount of internal metabolites pers of biomass, $x_i = \zeta_i/X$.

LA is produced because NADH cannot re-oxidize to NAD^+, although NAD^+ is required as an electron acceptor for the posterior oxidation of pyruvate. In such conditions, pyruvate is reduced to lactate by accepting electrons from NADH, thereby regenerating NAD^+, which is required to continue glycolysis [40]. Lactate is highly inhibitory on cell growth, thereby inducing a higher energy usage for maintenance (ATP), and energy is used for maintenance instead of the development and production of HA. As observed in Figure 5(e-1)–(e-6) the concentration of NADH is very high compared to NAD^+, which suggests that the high concentration of NADH could act as an inhibitor of growth and, therefore, of HA production.

Besides, the broth viscosity reaches as high as 400–500 mPas at 4–5 g/L HA, which causes poor mixing and a low oxygen mass transfer rate; thus, HA production is severely limited [9, 31] (Liu et al. 2011, Contreras-Mendoza et al., 2024).

NADH is a compound with antioxidant power that transfers hydrogen ions. Together with its oxidized version NAD^+, we find them at the bottom of Figure 5 (plots e-1 to e-6) (x_{NADH} and x_{NAD^+}). NADH shows a representative generation behavior in the three phases. At the same time, its homolog remains at constantly lower levels.

The specific reaction rates inside the microorganisms are defined as $\mu_i \equiv r_i/X$, $i = 1, 2, ..., 10$. In Figure 6(a-1)–(a-6), μ_1 represents the phosphorylation of glucose per biomass unit reaction, which releases energy; in all the experiments, it shows the same behavior, namely peaking in the exponential phase, and its activity grows as the extracellular glucose concentration increases. In the same graphics, μ_2 is drawn to represent the conversion of glucose into fructose; this is the only reaction that doesn't involve an energetic biomolecule. Its behavior begins with a fall followed by a slight increase in activity in the same phase as μ_1. This presumably indicates that the reaction that releases energy is more efficient than the one that only involves an enzymatic process.

In Figure 6(b-1)–(b-6), the reactions for μ_3, μ_4, and μ_5 are plotted together, which provides a comprehensive view of the glycolysis process towards LA. Both μ_3 and μ_4 require energy, with μ_3 also involving a reduction reaction, while μ_5 is the only reaction featuring oxidation. Their activity patterns are similar, with μ_4 exhibiting the highest activity, followed by μ_5 and μ_3 at the lower end. The series of reactions that μ_3 comprises may explain its lower activity than μ_5. To carry out these reactions, μ_3, similar to μ_4, consumes the energy produced in μ_1.

Figure 6(c-1)–(c-6) represent the production of HA; the μ_6 plot shows the conversion from glucose through glucuronic acid. These series of reactions realizes energy, and there is a reduction reaction process. Interestingly, despite the difference in extracellular glucose concentration, the peak of μ_6 is between 13 and 17 in all experiments, which indicates that its activity is not affected by the external glucose concentration. The activity of μ_7 is so low that it confirms that the production of HA is limited by the formation of N-Acetyl-D-Glucosamine, except for high initial concentrations of glucose, as shown in experiment 6, where the activity of μ_7 is much greater than in the rest of the experiments.

For HA production, namely μ_8, we see a greater variety of behaviors. In the first two experiments, at low glucose concentrations, it starts from a point where its activity declines until the exponential phase, which presents a peak that grows as the initial glucose concentration increases. For the intermediate experiments, a slight peak is observed in the latency phase, followed by a prominent peak in the exponential phase. In experiment 5, only a prominent peak in the exponential phase exceeds the activity of μ_6. Finally, in experiment 6, the graph starts from a high point from which it decays; in the change it appears to have a peak close to that of μ_6 between the exponential and stationary phase.

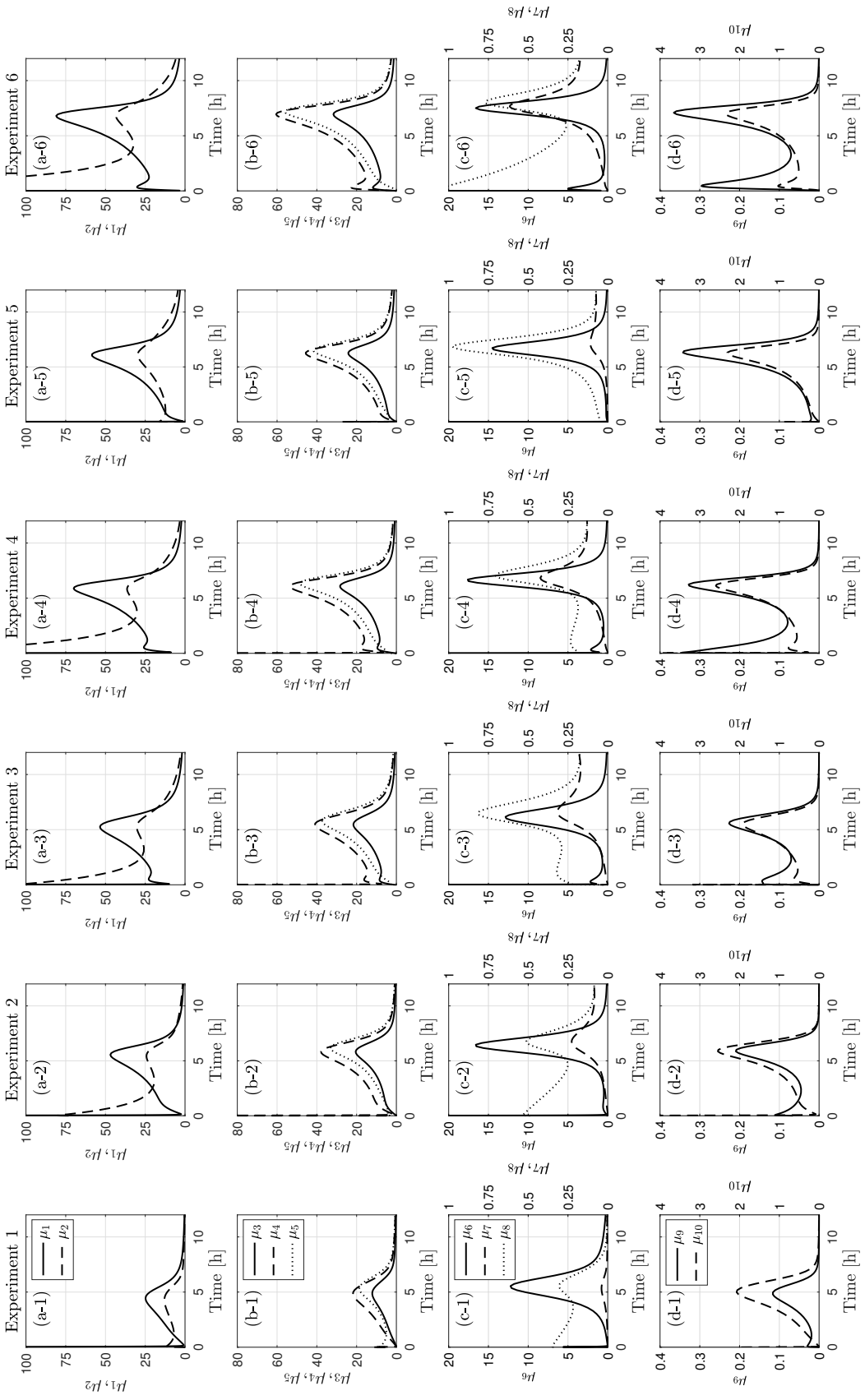

Figure 6. Specific reaction rates inside the microorganisms, $\mu_i \equiv r_i/X$, $i = 1, 2, ..., 10$.

The last plots of Figure 6 (from (d-1) to (d-6)) show the biomass formation represented for μ_9 and μ_{10}; both have a reduction reaction process that balances the oxidation process for LA production. A single peak can easily be perceived in the experimental phase of the first experiment. By increasing the glucose intake, the plots change significantly. In experiments 2–4, the activity of μ_9 starts at a high point, where it decreases with an increase in the exponential phase; on the contrary, μ_{10} starts at a low point, after twhich it can be compared to μ_9. For these two parameters, experiment 5 shows the same behavior, with the μ_9 peak being a little bit higher than μ_{10}. Finally, their behavior in experiment 6 is fascinating because both present two peaks of activity, one at the beginning of fermentation and another more pronounced in the exponential phase.

The objective of graphing μ against time is to obtain the value of μ_{max} and, on the other hand, to qualitatively observe whether any substrate or product exerts any inhibition phenomenon. The latter would be observed in the case of decreases in μ_{max}. In all the graphs, an increase in the maximum values of μ_{max} is generally observed when the glucose concentration increases, which does not cause any type of inhibition on the components involved. In the cases where the initial lines that descend are observed (Figure 6(a-3), (a-4), (a-6), (c-1), (c-2), (c-6), (d-2), (d-3), (d-4)), it would indicate that a second substrate is finishing its degradation. These substrates often exert regulatory phenomena, which causes the substrate of interest to degrade until this second substrate does so. This is different here. In Figure 6(d-6), the presence of a second substrate related to μ_9 is observed.

4. Conclusions

In this study, we introduced and validated a mathematical model that combined kinetic and metabolic pathways to predict the dynamic behavior of biomass, glucose, HA, and LA concentrations in fermentations of *Streptococcus equi* subsp. *zooepidemicus*. As depicted in Figure 2, the HA production is a complex process that involves several steps inside microorganisms. However, we proposed a simplified version of this metabolic pathway, depicted in Figure 3, where intermediate reactions were grouped to obtain overall reactions that contained bifurcation points for some key reactants or products. The proposed approach allows us to consider the qualitative dynamic behavior of key internal unmeasured metabolites associated with glycolysis, biomass growth, HA production, and cellular metabolic regulation. These internal metabolites are the intracellular molar concentrations of glucose, G6P, F6P, PEP, PYR, UDP-N-acetylglucosamine, UDP-Glucoronic acid, ATP, ADP, NADH, and NAD^+.

As seen in Figure 4, the model's predictions aligned well with the experimental data, and the variations for the internal metabolites and their reaction rates can be used to understand how different initial concentrations of glucose influence the metabolic pathways. In particular, energetic and oxidative agents such as ATP/ADP and NADH/NAD^+ play a crucial role in cellular metabolic regulation. Finally, the proposed model can be applied to improve existing HA production processes and to propose new processes configurations and control strategies to optimize HA production.

Use of AI tools declaration

The authors declare they have not used Artificial Intelligence (AI) tools in the creation of this article.

Acknowledgments

J. P. García-Sandoval acknowledges the grant (SNII-43658) provided by Science, Humanities, Technology and Innovation Agency (SECIHTI) of Mexico through the program of the National Researches System (SNII). A. Galindo acknowledges the grant (No. 863553) provided by SECIHTI through the program of National Scholarships for Postgraduate Studies.

Conflict of interest

The authors declare there is no conflict of interest.

References

1. Y. Xue, K. Ucieklak, S. Gohil, T. Niedziela, G. Nestor, C. Sandström, Metabolic labeling of hyaluronan: Biosynthesis and quantitative analysis of 13C,15N-enriched hyaluronan by NMR and MS-based methods, *Carbohydr. Res.*, **531** (2023), 108888. https://doi.org/10.1016/j.carres.2023.108888
2. T. T. Vu, M. Gulfam, S. H. Jo, A. Rizwan, S. B. Joo, B. Lee, et al., The effect of molecular weight and chemical structure of cross-linkers on the properties of redox-responsive hyaluronic acid hydrogels, *Int. J. Biol. Macromol.*, **238** (2023), 124285. https://doi.org/10.1016/j.ijbiomac.2023.124285
3. S. Afrasiabi, F. S. A. Zanjani, G. Ahmadian, R. A. Cohan, M. Keramati, The effect of manipulating glucuronic acid biosynthetic pathway in Bacillus subtilis strain on hyaluronic acid production, *AMB Express*, **13** (2023), 1–12. https://doi.org/10.1186/s13568-023-01567-2
4. F. Jabbari, V. Babaeipour, S. Saharkhiz, Comprehensive review on biosynthesis of hyaluronic acid with different molecular weights and its biomedical applications, *Int. J. Biol. Macromol.*, **240** (2023), 124484. https://doi.org/10.1016/j.ijbiomac.2023.124484
5. P. Rampratap, A. Lasorsa, B. Perrone, P. C. van der Wel, M. T. Walvoort, Production of isotopically enriched high molecular weight hyaluronic acid and characterization by solid-state NMR, *Carbohydr. Polym.*, **316** (2023), 121063. https://doi.org/10.1016/j.carbpol.2023.121063
6. Y. Luo, J. Tan, Y. Zhou, Y. Guo, X. Liao, L. He, et al., From crosslinking strategies to biomedical applications of hyaluronic acid-based hydrogels: A review, *Int. J. Biol. Macromol.*, **231** (2023), 123308. https://doi.org/10.1016/j.ijbiomac.2023.123308
7. M. Bhattacharyya, H. Jariyal, A. Srivastava, Hyaluronic acid: More than a carrier, having an overpowering extracellular and intracellular impact on cancer, *Carbohydr. Polym.*, **317** (2023), 121081. https://doi.org/10.1016/j.carbpol.2023.121081
8. D. A. Flores-Méndez, C. Pelayo-Ortiz, Á. d. J. Martínez Gómez, G. Toriz, G. M. Guatemala-Morales, R. I. Corona-González, Evaluation of agave tequilana by-products for microbial production of hyaluronic acid, *Bioresour. Technol. Rep.*, **21** (2023), 101366. https://doi.org/10.1016/j.biteb.2023.101366

9. J. Contreras Mendoza, E. Arriola Guevara, L. A. Suarez Hernández, G. Toriz, G. M. Guatemala-Morales, R. I. Corona-González, Evaluation of mango residues to produce hyaluronic acid by Streptococcus zooepidemicus, *Folia Microbiol.*, **69** (2024), 847–856. https://doi.org/10.1007/s12223-023-01123-2

10. N. I. Abdullah Thaidi, R. Mohamad, H. Wasoh, M. R. Kapri, A. B. Ghazali, J. S. Tan, et al., Development of in situ product recovery (ISPR) system using amberlite IRA67 for enhanced biosynthesis of hyaluronic acid by Streptococcus zooepidemicus, *Life*, **13** (2023), 558. https://doi.org/10.3390/life13020558

11. P. Shukla, R. Sinha, S. Anand, P. Srivastava, A. Mishra, Tapping on the potential of hyaluronic acid: from production to application, *Appl. Biochem. Biotechnol.*, **195** (2023), 7132–7157. https://doi.org/10.1007/s12010-023-04461-6

12. D. A. Flores-Méndez, J. R. Ramos-Ibarra, G. Toriz, E. Arriola-Guevara, G. Guatemala-Morales, R. I. Corona-González, Bored coffee beans for production of hyaluronic acid by Streptococcus zooepidemicus, *Fermentation*, **7** (2021), 121. https://doi.org/10.3390/fermentation7030121

13. A. Fallacara, E. Baldini, S. Manfredini, S. Vertuani, Hyaluronic acid in the third millennium, *Polymers*, **10** (2018), 701. https://doi.org/10.3390/polym10070701

14. M. J. Wade, Not just numbers: Mathematical modelling and its contribution to anaerobic digestion processes, *Processes*, **8** (2020), 888. https://doi.org/10.3390/pr8080888

15. G. Bastin, D. Dochain, Chapter 1 - dynamical models of bioreactors, in *On-line Estimation and Adaptive Control of Bioreactors* (eds. G. Bastin and D. Dochain), Process Measurement and Control, Elsevier, Amsterdam, (1990), 1–82.

16. S. Rathinavelu, S. S. Pavan, S. Sivaprakasam, Hybrid model-based framework for soft sensing and forecasting key process variables in the production of hyaluronic acid by Streptococcus zooepidemicus, *Biotechnol. Bioprocess Eng.*, **28** (2023), 203–214. https://doi.org/10.1007/s12257-022-0247-x

17. M. Albino, C. L. Gargalo, G. Nadal-Rey, M. O. Albaek, U. Krühne, K. Gernaey, Hybrid modeling for on-line fermentation optimization and scale-up: A review, *Processes*, **12** (2024), 1635.

18. A. K. Gombert, J. Nielsen, Mathematical modelling of metabolism, *Curr. Opin. Biotechnol.*, **11** (2000), 180–186. https://doi.org/10.1016/S0958-1669(00)00079-3

19. M. M. Don, N. F. Shoparwe, Kinetics of hyaluronic acid production by Streptococcus zooepidemicus considering the effect of glucose, *Biochem. Eng. J.*, **49** (2010), 95–103. https://doi.org/10.1016/j.bej.2009.12.001

20. J. A. Vázquez, M. I. Montemayor, J. Fraguas, M. A. Murado, High production of hyaluronic and lactic acids by streptococcus zooepidemicus in fed-batch culture using commercial and marine peptones from fishing by-products, *Biochem. Eng. J.*, **44** (2009), 125–130. https://doi.org/10.1016/j.bej.2008.11.007

21. I. R. Amado, J. A. Vázquez, L. Pastrana, J. A. Teixeira, Microbial production of hyaluronic acid from agro-industrial by-products: Molasses and corn steep liquor, *Biochem. Eng. J.*, **117** (2017), 181–187. https://doi.org/10.1016/j.bej.2016.09.017

22. A. Ozcan, M. Germec, I. Turhan, Optimization and kinetic modeling of media composition for hyaluronic acid production from carob extract with Streptococcus zooepidemicus, *Bioprocess. Biosyst. Eng.*, **45** (2022), 2019–2029. https://doi.org/10.1007/s00449-022-02806-9

23. S. G. Rohit, P. K. Jyoti, R. R. T. Subbi, M. Naresh, S. Senthilkumar, Kinetic modeling of hyaluronic acid production in palmyra palm (Borassus flabellifer) based medium by Streptococcus zooepidemicus MTCC 3523, *Biochem. Eng. J.*, **137** (2018), 284–293. https://doi.org/10.1016/j.bej.2018.06.011

24. L. Liu, M. Wang, G. Du, J. Chen, Enhanced hyaluronic acid production of streptococcus zooepidemicus by an intermittent alkaline-stress strategy, *Lett. Appl. Microbiol.*, **46** (2008), 383–388. https://doi.org/10.1111/j.1472-765X.2008.02325.x

25. D. A. Flores-Méndez, M. Granados-Vallejo, G. M. Guatemala-Morales, R. I. Corona-González, C. Pelayo-Ortíz, E. Arriola-Guevara, Influence of initial glucose and lactic acid concentration on hyaluronic acid production by Streptococcus zooepidemicus: Kinetic and modeling, *Biochem. Eng. J.*, **205** (2024), 109262. https://doi.org/10.1016/j.bej.2024.109262

26. L. Liu, J. Sun, W. Xu, G. Du, J. Chen, Modeling and optimization of microbial hyaluronic acid production by streptococcus zooepidemicus using radial basis function neural network coupling quantum-behaved particle swarm optimization algorithm, *Biotechnol. Progr.*, **25** (2009), 1819–1825. https://doi.org/10.1002/btpr.278

27. M. J. Cooney, L. T. Goh, P. L. Lee, M. R. Johns, Structured model-based analysis and control of the hyaluronic acid fermentation by streptococcuszooepidemicus: Physiological implications of glucose and complex-nitrogen-limited growth, *Biotechnol. Progr.*, **15** (1999), 898–910. https://doi.org/10.1021/bp990078n

28. M. V. Shah, S. S. Badle, K. Ramachandran, Hyaluronic acid production and molecular weight improvement by redirection of carbon flux towards its biosynthesis pathway, *Biochem. Eng. J.*, **80** (2013), 53–60. https://doi.org/10.1016/j.bej.2013.09.013

29. B. F. Chong, L. K. Nielsen, Aerobic cultivation of Streptococcus zooepidemicus and the role of NADH oxidase, *Biochem. Eng. J.*, **16** (2003), 153–162. https://doi.org/10.1016/S1369-703X(03)00031-7

30. H. J. Gao, G. C. Du, J. Chen, Analysis of metabolic fluxes for hyaluronic acid (HA) production by Streptococcus zooepidemicus, *World J. Microbiol. Biotechnol.*, **22** (2006), 399–408. https://doi.org/10.1007/s11274-005-9047-7

31. L. Liu, Y. Liu, J. Li, G. Du, J. Chen, Microbial production of hyaluronic acid: Current state, challenges, and perspectives, *Microb. Cell Fact.*, **10** (2011), 1–9. https://doi.org/10.1186/1475-2859-10-99

32. G. Bayon-Vicente, L. Toubeau, M. Gilson, G. Gégo, N. Landgey, S. Krings, et al., Metabolic pathways to sustainability: Review of purple non-sulfur bacteria potential in agri-food waste valorization, *Front. Bioeng. Biotechnol.*, **13** (2025), 1529032. https://doi.org/10.3389/fbioe.2025.1529032

33. Z. Y. Yao, J. S. Gong, Y. R. Liu, J. Y. Jiang, Y. S. Zhang, C. Su, et al., Genetic variation reveals the enhanced microbial hyaluronan biosynthesis via atmospheric and room temperature plasma, *Carbohydr. Polym.*, **312** (2023), 120809. https://doi.org/10.1016/j.carbpol.2023.120809

34. S. Klamt, H. Grammel, R. Straube, R. Ghosh, E. Gilles, Modeling the electron transport chain of purple non-sulfur bacteria, *Mol. Syst. Biol.*, **4** (2008), 156.

35. J. C. Lagarias, J. A. Reeds, M. H. Wright, P. E. Wright, Convergence properties of the Nelder–Mead simplex method in low dimensions, *SIAM J. Optim.*, **9** (1998), 112–147. https://doi.org/10.1137/S1052623496303470

36. A. Constantinides, N. Mostoufi, *Numerical Methods for Chemical Engineers with MATLAB applications*, Prentice Hall PTR, 2000.

37. A. Buchholz, J. Hurlebaus, C. Wandrey, R. Takors, Metabolomics: Quantification of intracellular metabolite dynamics, *Biomol. Eng.*, **19** (2002), 5–15. https://doi.org/10.1016/S1389-0344(02)00003-5

38. E. Zborníková, Z. Knejzlík, V. Hauryliuk, L. Krásný, D. Rejman, Analysis of nucleotide pools in bacteria using HPLC-MS in HILIC mode, *Talanta*, **205** (2019), 120161. https://doi.org/10.1016/j.talanta.2019.120161

39. C. G. Boeriu, J. Springer, F. K. Kooy, L. A. M. van den Broek, G. Eggink, Production methods for hyaluronan, *Int. J. Carbohydr. Chem.*, **2013** (2013), 624967. https://doi.org/10.1155/2013/624967

40. M. Cox, D. Nelson, *Lehninger Principles of Biochemistry: International Edition*, Macmillan Learning, 2021.

AIMS Press